Multi-scale Circular Conebeam Interior Tomography using Bedrosian Identity: Verification with Real Data

Yo Seob Han[1], Minji Lee[1], John Paul Ward[2], Michael Unser[3], Seungryoung Cho[4] and Jong Chul Ye[1,*]

***Abstract*—Circular trajectory is quite often used in conebeam CT (CBCT) such as C-arm CT, dental CT and so on. However, if the cone angle is wide, the FDK algorithm suffers from conebeam artifacts. Moreover, it exhibits severe truncation artifacts if the detector is truncated in transverse-ways. To mitigate these artifacts, we propose a reconstruction method that consists of two steps: multi-scale interior tomography using 1D TV in both horizontal and vertical virtual chord lines, which is followed by spectral blending in Fourier domain. For spectral blending, we develop a Fourier domain analysis technique to identify the missing frequency regions and design a bow tie window for weighting. Experimental results with a real head phantom confirm that the proposed method significantly improves the reconstruction quality and reduces the computational time significantly.**

***Index Terms*—Conebeam artifact, Interior tomography, Bedrosian theorem, Multiscale decomposition, Spectral Blending.**

I. Introduction

CIRCULAR CBCT trajectory has been widely used in practice since the trajectory can be easily implemented in hardware compared to other geometries such as helical [1] or saddle [2] trajectories. In the circular trajectory, the FDK algorithm is the de facto standard, but it suffers from the conebeam artifacts as the cone angle increases. These artifacts become more severe when only part of detector is used for imaging the region-of-interior (ROI) to reduce the radiation dose.

Specifically, interior tomography approaches reduce the x-ray dose by preventing x-ray illumination outside of the ROI. However, due to the detector truncation, the conventional filtered back projection type algorithm cannot be used. To address this problem, the authors in [3] showed that if the object is essentially piecewise constant, then ROI can be solved uniquely and stably via the total variation (TV) minimization. However, this methods requires 2D or 3D total variation minimization and iterative applications of forward and backward projections, which is computationally very expensive.

[1]Bio Imaging & Signal Processing Lab., Dept. of Bio and Brain Engineering, Korea Advanced Institute of Science & Technology (KAIST), 291 Daehak-ro, Yuseong-gu, Daejon, Korea. (minjilee@kaist.ac.kr, hanyoseob@kaist.ac.kr, jong.ye@kaist.ac.kr).

[2]Department of Mathematics, University of Central Florida, Orlando, FL 32815. (john.ward@ucf.edu).

[3]Biomedical Imaging Group, École Polytechnique Fédérale de Lausanne (EPFL), CH-1015, Lausanne, Switzerland. (michael.unser@epfl.ch).

[4]Medical Imaging & Radiotherapeutic Lab., Dept. of Bio and Brain Engineering, Korea Advanced Institute of Science & Technology (KAIST), 291 Daehak-ro, Yuseong-gu, Daejon, Korea. (scho@kaist.ac.kr).

In interior tomography problems from circular trajectory, two types of artifacts reside: one from truncated detectors and the other from missing frequency regions. To address the first artifact, our group recently proposed the multi-scale interior tomography algorithm using 1D TV [4]. Then, to reduce the second type artifacts, we also extended the Fourier blending idea proposed for half-scan FBP algorithm [5] to our multi-scale interior tomography approach, and provided a novel Fourier domain two-way weighting scheme [4]. Unlike the original Fourier blending idea in [5], our method is based on rigorous analysis of Fourier components. The resulting algorithm is computationally so efficient that it can be easily used in a clinical environment.

The main goal of this paper is, therefore, to demostrate the effectiveness of this algorithm using real data. For this, we first review the recent theory of multi-scale circular conebeam interior tomography using Bedrosian identity and spectal blending [4] and provide experimental results using real data.

II. Thoery

A. Conebeam artifact problem

1) Fourier analysis of DBP on virtual chord lines: In the 3-D CBCT problem, let the variables $\boldsymbol{\theta}$ denote a vector on the unit sphere $\mathbb{S}^2 \in \mathbb{R}^3$. Then, the x-ray transform is formally define as

$$D_f(\mathbf{a}, \boldsymbol{\theta}) = \int_0^\infty f(\mathbf{a} + t\boldsymbol{\theta}) dt \ , \tag{1}$$

where f corresponds to the linear attenuation coefficients and $\boldsymbol{\theta} \in \mathbb{S}^2$ denotes the x-ray photon propagation direction and $\mathbf{a} \in \mathbb{R}^3$ refers the x-ray source location in a actual source trajectory $\mathbf{a}(\lambda), \lambda \in [\lambda_{\min}, \lambda_{\max}]$.

For the given source trajectory $\mathbf{a}(\lambda)$, we now define the *differentiated backprojection (DBP)*:

$$g(\mathbf{x}) \quad = \quad \int_{\lambda^-}^{\lambda^+} d\lambda \frac{1}{\|\mathbf{x} - \mathbf{a}(\lambda)\|} \frac{\partial}{\partial \nu} D_f\left(\mathbf{a}(\nu), \boldsymbol{\theta}\right)\big|_{\nu=\lambda} \tag{2}$$

where $[\lambda^-, \lambda^+] \subset [\lambda_{\min}, \lambda_{\max}]$ denotes the appropriate intervals from the source segments between $\lambda_{\min}$ and $\lambda_{\max}$, and $1/\|\mathbf{x} - \mathbf{a}(\lambda)\|$ denotes the distance weighting. The chord line on the DBP data can be representated as a Hilbert transform relationship [1], [6], [7]. Unfortunately, in CBCT, the Hilbert transform relationship is established only on the actual chord line. As our novel contribution, we generalized the Hilbert transform relationship from the actual chord line to a virtual chord line [4].

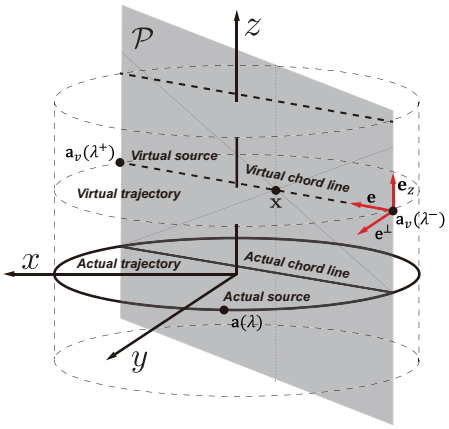

Fig. 1. Source trajectories and virtual chord lines. The dark circle is an actual trajectory and the dark line is an actual chord line. The set of gray-dot circle are virtual trajectory and the dark-dot line is a virtual chord line.

The virtual coordinate system can be explained by three unit vectors which are the z-axis $\mathbf{e}_z$, the chord line direction (i.e., filtering direction) $\mathbf{e}$, and their perpendicular axis $\mathbf{e}^\perp$. Using the coordinate system, a new coordinate (x', y', z) is representated from a primary Cartesian coordinate such that

$$\mathbf{x} = x'\mathbf{e} + y'\mathbf{e}^\perp + z\mathbf{e}_z \ . \tag{3}$$

At the new coordinate, the corresponding spatial frequency is defined by $(w_{x'}, w_{y'}, w_z)$. Then, we have the following gerenalized Hilbert transform relationship.

Theorem II.1. [4] Let the source trajectory $\mathbf{a}(\lambda), \lambda \in [\lambda^-, \lambda^+]$ have no discontinuities. Suppose, furthermore, position $\mathbf{x}$ is on the viritual chord line that connects the two virtual source positions $\mathbf{a}_v(\lambda^-)$ and $\mathbf{a}_v(\lambda^+)$, and has the coordinate values (x', y', z) on the virtual chord line coordinate system (3). Then, the differentiated backprojection data in (2) can be represented as

$$g(\mathbf{x}) = \frac{1}{2\pi}\int_{-\infty}^{\infty} d\omega_{x'}\ \hat{\phi}(\omega_{x'}, y', z) j\,\mathrm{sgn}(\omega_{x'}) e^{j\omega_{x'}x'} \tag{4}$$

where

$$\hat{\phi}(\omega_{x'}, y', z) := \frac{1}{(2\pi)^2}\int d\omega_{x'}\int_{\omega_z \in \{(\omega_{x'},\omega_{y'},\omega_z)\notin\mathcal{N}(z)\}} d\omega_z \\ \hat{f}(\omega_{x'}, \omega_{y'}, \omega_z) e^{j(y'\omega_{y'}+z\omega_z)} \ ,$$

and the missing frequency set $\mathcal{N}(z)$ on z is given by

$$\mathcal{N}(z) = \left\{(\omega_{x'}, \omega_{y'}, \omega_z) \mid -A \le \frac{\omega_{x'}}{z\omega_z} \le B\right\}, \tag{5}$$

where

$$A = \frac{1}{x' + \sqrt{R^2 - (y')^2}},\ B = \frac{1}{\sqrt{R^2 - (y')^2} - x'}.$$

which trivially becomes an empty set when $z = 0$.

2) Missing frequency regions: Thanks to Theorem II.1, we can identify the missing frequency region. Fig. 2 shows various missing frequency regions depends on the filtering direction. If all of the chord lines head for the horizontal direction (blue line at Fig. 2(a)), then the missing frequency region for a given z can be written as

$$\left\{(\omega_x, \omega_y, \omega_z) \mid -\frac{z\omega_z}{x + \sqrt{R^2 - y^2}} \le \omega_x \le \frac{z\omega_z}{\sqrt{R^2 - y^2} - x}\right\}$$

, where $z\omega_z \le 0$; on the contrary, for the vertical direction (red line at Fig. 2(b)), the missing frequency region can be explained such that

$$\left\{(\omega_x, \omega_y, \omega_z) \mid -\frac{z\omega_z}{y + \sqrt{R^2 - x^2}} \le \omega_y \le \frac{z\omega_z}{\sqrt{R^2 - x^2} - y}\right\}$$

.

The missing frequency region is illustrated in Fig. 2(b)(c) for $x \ll z, y \ll z$, respectively. In addition, Fig. 2(d)(e) represents the missing frequency regions related to the diagonal filtering directions.

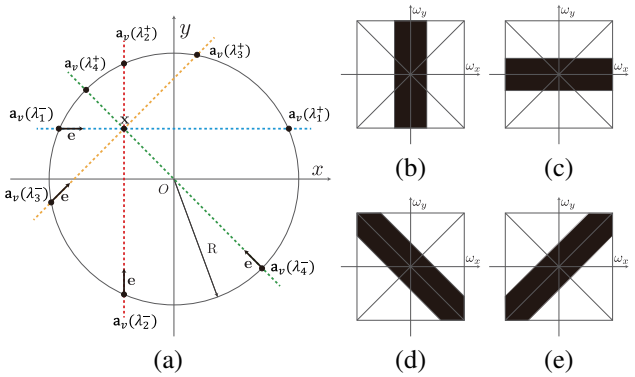

Fig. 2. The missing frequency region. (a) The top view of a point $\mathbf{x} = (x, y, z)$ and an source trajectory. The blue line indicates the horizontal directional virtual chord line between $\mathbf{a}_v(\lambda_1^-)$ and $\mathbf{a}_v(\lambda_1^+)$ and the red line denotes the vertical directional virtual chord lines between $\mathbf{a}_v(\lambda_2^-)$ and $\mathbf{a}_v(\lambda_2^+)$. (b)(c) The missing frequency region for horizontal and vertical directions, respectively. (d) (e) The missing frequency region for the diagonal directional virtual chord lines that correspond to the yellow and green lines, respectively.

B. Multi-scale Interior Tomography using Bedrosian Identity

In interior tomography problems, an available DBP data on a virtual chord line is truncated within FOV $x_\pi \in (e1, e2)$. Accordingly, when Hilbert transform is applied to the truncated data, we can expect truncation artifacts since there exists a null space:

$$\mathcal{H}h_{\mathcal{N}}(x_\pi) \quad = \quad 0, \quad \text{where} \quad x_\pi \in (e1, e2). \tag{6}$$

Here

$$h_{\mathcal{N}}(x_\pi) \quad = \quad \frac{1}{\pi}\int_{\mathbb{R}\setminus(e1,e2)} dx'_\pi\ \frac{\psi_\pi(x'_\pi)}{x'_\pi - x_\pi}, \tag{7}$$

for some function $\psi_\pi(x)$. Thus, we are interested in imposing 1D TV to correct any data $h_{\mathcal{N}}(x_\pi)$ belong to the null space.

By decomposing interior tomgoraphy problems based on the 1D TV formulations, the computational cost is much lower than it is for high-dimensional TV [3], [8], [9]. Moreover, we can significantly reduce the computational complexity based on the Bedrosian identity of Hilbert transform.

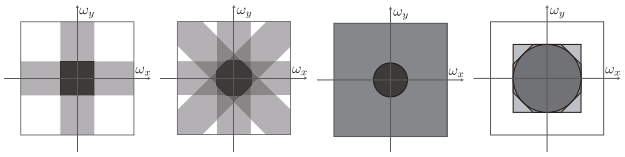

Fig. 3. The common missing frequency region according to the filtering directions. (a), (b), and (c) indicate the missing frequency region according to the number of missing frequency regions with different filtering directions. The dark region denotes a common missing frequency region, respectively. (d) Overlapped illustration of the common missing frequency regions.

Theorem II.2. (see [10]) *Let $w, f \in L_2(\mathbb{R})$ be low-pass and high-pass signals such that the Fourier transform of $w(x)$ vanishes for $|\omega| > \omega_0$, with $\omega_0 > 0$, and the Fourier transform of $f(x)$ vanishes for $|\omega| < \omega_0$. Then, we have*

$$\mathcal{H}\{w(x)f(x)\} = w(x)\mathcal{H}\{f(x)\} \ . \tag{8}$$

Accordingly, the interior tomography problem is formulated as

$$\min_{f_L} \|f_L\|_{TV(\mathrm{L};E)} \quad \text{subject to} \quad g = \mathcal{H}(f_L + f_H) \ . \tag{9}$$

where f_L and f_H denote the low and high freqeuncy component of a object f, respectively. By solving Eq. (9), the low freqeuncy component $f_L(x)$ is reconstructed under TV constraint. Moreover, it is possible to reconstruct low-resolution image in the down-sampled domain, so the computational bunden is significantly reduced. From the reconstruncted signal $f_L(x)$, the residual signal $g_H(x)$ is extracted by substracting $\mathcal{H}f_L(x)$ from $g(x)$. If $g_H(x)$ does not overlap with the spectral band-width of the truncation window, then Theorem II.2 is satisfied, so, $f_H(x)$ is directly calculated by

$$f_H(x) = \frac{-\mathcal{H}\{w(x)g_H(x)\}}{w(x)}, \quad x \in E. \tag{10}$$

The multiscale decomposition method is summarized in Fig. 4.

C. Conebeam artifact reduction using spectral blending

However, the recovered signal is not the exact solution due to the missing frequency regions. Indeed, the best signal we can expect is that the signals with missing frequency components as shown in Fig. 2. Therefore, to minimize the cone beam artifacts that are recovered from the interior tomography algorithm, we need spectral blending that optimally combines the interior tomography reconstruction in multiple filtering directions so that the resulting missing frequency components can be reduced to those of Fig. 3. Moreover, based

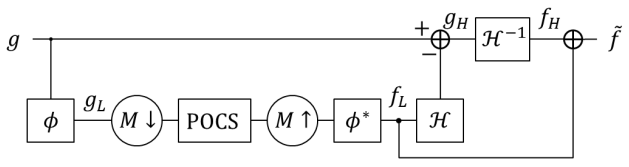

Fig. 4. Flowchart of the proposed multiscale reconstruction approach for interior tomography problem.

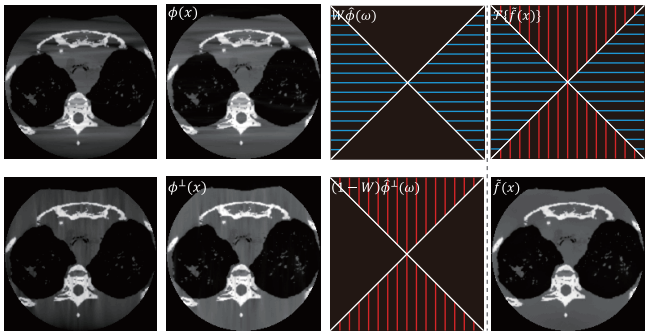

Fig. 5. ROI tomography reconstruction results using (a) BPF, (b) the proposed multiscale reconstruction method along horizontal ($\phi(x)$) and vertical ($\phi^{\perp}(x)$) filter directions, and (c) their the spectral blending results from the two filtering directions.

on Fig. 3, the size of the missing frequency regions from two orthogonal filtering directions is still comparable to that of multiple filtering directions. Since additional filtering direction requires additional applications of iterative interior topography algorithm, the computational complexity increases; so this paper just utilities the two filtering directions along x- and y- axis and apply the optimal spectral blending.

More specifically, as shown in the Fig. 3, it is possible to minimize the missing frequency region by blending appropriate frequency components of the reconstruction from the two orthogonal filtering directions. The shape of missing frequency region is described as Fig. 2(b) owing to the horizontal filtering direction, then it can be minimized by applying the row-wise bow tie window like Fig. 5(c) blue window. On the contrary, the shape is described as Fig. 2(c) owing to the vertical filtering direction, then it can be also minimized by applying the column-wise bow tie window like Fig. 5(c) red window. Finally, by blending both the weighted spectrums, the missing frequency region can be minimized in the 2D Fourier domain in each slice. Therefore, we apply 2D Fourier transform for each z-slice and use the spectral blending, which significantly reduces the computational burden. The concept of spectral blending simply is illustrated in Fig. 5. The multiscale decomposition interior tomography algorithm is used for both horizontal and vertical directions, respectively. Then, using spectral weighting with a bow-tie window, they are blended into one image.

III. Results

The reconstruction domain resolution of the real head phantom was $512 \times 512 \times 512$ voxles with voxel size $0.589 \times 0.589 \times 0.684$ mm^3, and the phantom size is $(-150, 150) \times (-150, 150) \times (-175, 175)$ mm^3. The resolution of the detector is 1024×250 array matrix with detector pitch of 0.4×0.4 mm^2 and the number of views is 720. The distance from source to rotation axis is 1700 mm, and the distance from source to detector is 2250 mm. The radius of FOV was about 36 mm. Since a transverse-ways offset is applied as 5.0 pitch, when the projection data was acquired, the ROI of the reconstructed head phantom is biased toward the right-bottom side.

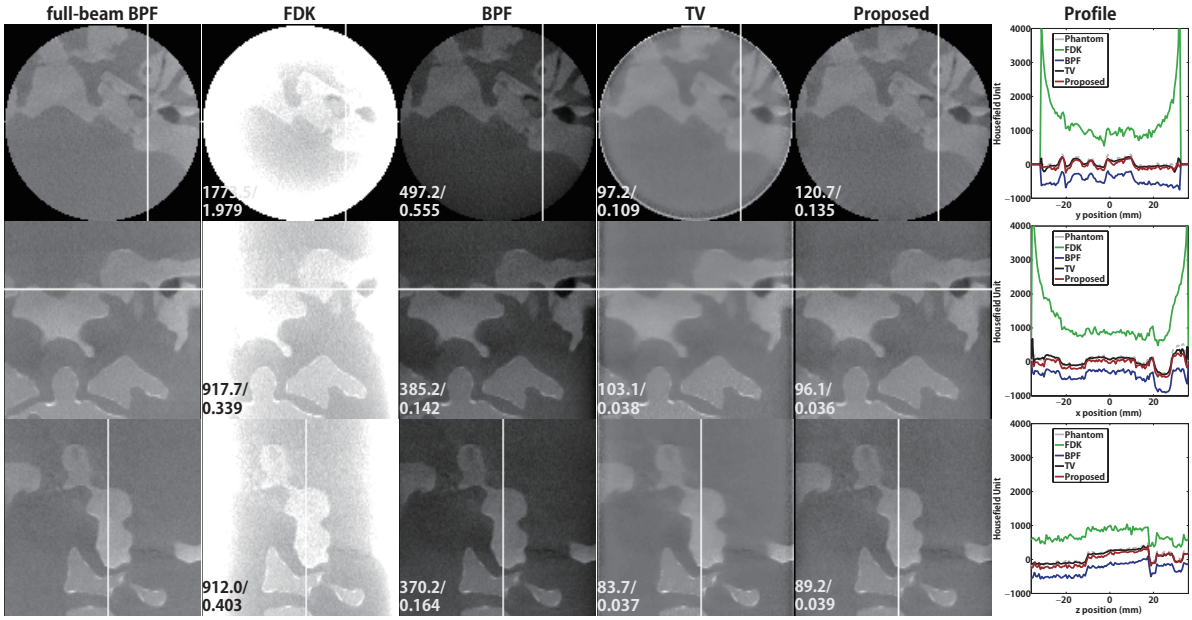

Fig. 6. The reconstruction results of real head phantom. From top to bottom, the each row denotes the cross section for the transection at $z = -11.3$ mm (*i.e.* off-mid-plane), the coronal at $y = -3.8$ mm, and the sagittal at $x = -0.9$ mm. The profiles corresponds to the CT numbers along the white lines of the reconstructed results. The profiles of full-beam BPF, FDK, BPF, TV and proposed method are represented by gray-dot, green, blue, and red, respectively.

In Fig. 6, reconstruction results for a real head phantom are shown in the region $(-36, 36) \times (-36, 36) \times (-36, 36)$ mm^3. Although the proposed method is truncated as about 70%, the results in Fig. 6 are very similar to that of the full-beam result. Unlike the TV reconstruction, the noise textures could be recovered by the proposed method, and confirmed that the algorithm does not result in unnatural smoothing. This is because TV is only applied at the low frequency reconstruction, and the high frequency reconstruction is done an using analytic formula.

When the computation time is compared between the proposed and conventional iterative (TV) method, a performance of reconstruction is 2.2 slice/sec for the proposed method, however, in the conventional case, the performance is 0.0667 slice/sec. This shows that the proposed method is 34.3 times accelerated over the conventional.

IV. Conclusion

In this paper, we provided a novel analysis of the missing frequency region using Fourier domain analysis, which is distinct from the Radon domain approach in [5]. Based on the analysis, an optimal spectral blending scheme that weights the reconstruction from two orthogonal filtering directions was proposed. We further demonstrated that the DBP data from the circular cone beam data has a similar Hilbert transform relationship on virtual chord lines, but the content is different owing to the missing frequency regions. Accordingly, our algorithm consisted of two step reconstruction procedure: first, the multiscale decomposition interior tomography algorithm using 1D TV penalty on the virtual chord lines, which is followed by spectral blending of a two reconstructions from horizontal and vertical filtering directions. The proposed method provided the reconstruction result with significantly reduced conebeam and missing frequency artifacts. Furthermore, all the processing were done in 1D virtual chord lines, which significantly reduces the computational complexity.

This work was supported by Korea Science and Engineering Foundation by Grant NRF- 2014R1A2A1A11052491.

References

[1] Y. Zou and X. Pan, "Exact image reconstruction on PI-lines from minimum data in helical cone-beam CT," *Physics in Medicine and Biology*, vol. 49, no. 6, pp. 941, 2004.

[2] Haiquan Yang, Meihua Li, Kazuhito Koizumi, and Hiroyuki Kudo, "Exact cone beam reconstruction for a saddle trajectory," *Physics in Medicine and Biology*, vol. 51, no. 5, pp. 1157–1172, 2006.

[3] Hengyong Yu and Ge Wang, "Compressed sensing based interior tomography," *Physics in Medicine and Biology*, vol. 54, no. 9, pp. 2791–2805, 2009.

[4] Minji Lee, Yoseob Han, John Paul Ward, Michael Unser, and Jong Chul Ye, "Interior tomography using 1d generalized total variation. part ii: Multiscale implementation," *SIAM Journal on Imaging Sciences*, vol. 8, no. 4, pp. 2452–2486, 2015.

[5] JD Pack, Z Yin, K Zeng, and BE Nett, "Mitigating cone-beam artifacts in short-scan CT imaging for large cone-angle scans," *Fully 3D Image Reconstruction in Radiology and Nuclear Medicine*, pp. 307–310, 2013.

[6] Jed D Pack and Frédéric Noo, "Cone-beam reconstruction using 1D filtering along the projection of M-lines," *Inverse Problems*, vol. 21, no. 3, pp. 1105–1120, 2005.

[7] Y. Zou and X. Pan, "Image reconstruction on PI-lines by use of filtered backprojection in helical cone-beam CT," *Physics in Medicine and Biology*, vol. 49, no. 12, pp. 2717, 2004.

[8] J. Yang, H. Yu, M. Jiang, and G. Wang, "High-order total variation minimization for interior tomography," *Inverse Problems*, vol. 26, no. 3, pp. 035013, 2010.

[9] Weimin Han, Hengyong Yu, and Ge Wang, "A general total variation minimization theorem for compressed sensing based interior tomography," *Journal of Biomedical Imaging*, vol. 2009, pp. 21, 2009.

[10] Frederick W King, *Hilbert transforms*, vol. 2, Cambridge University Press Cambridge, UK, 2009.